Alternating Crystalline Lamellar Structures from Thermodynamically Miscible Poly(ε-caprolactone) H/D Blends

Lengwan Li [a, b, d], Matthias M.[1] L. Arras [c], Tianyu Li [b, e], Wei Li [b], Dongsook Chang [b], Jong K. Keum [b,c], Peter V. Bonnesen [b], Shuo Qian [c], Xiangfang Peng [a]*, Byeongdu Lee [f], Kunlun Hong [b, d]*

[a] *The Key Laboratory of Polymer Processing Engineering of Ministry of Education, South China University of Technology, Guangzhou 510640, China*

[b] *Center for Nanophase Materials Sciences and* [c] *Neutron Scattering Division, Oak Ridge National Laboratory, Oak Ridge, Tennessee 37831, USA*

[d] *Department of Chemical and Biomolecular Engineering and* [e] *Department of Materials Science and Engineering, University of Tennessee, Knoxville, Tennessee 37996, USA*

[f] *X-ray Science Division, Argonne National Laboratory, Argonne, Illinois 60439, USA*

Correspondence to:

Xiangfang Peng (pmxfpeng@scut.edu.cn);

Kunlun Hong (hongkq@ornl.gov).

Abstract:

Thermodynamic interaction and non-isothermal crystallization behaviors in a series of protiated (H-) and deuterated (D-) poly (ε-caprolactone) (PCL) blends have been systematically investigated. The blends were thermodynamically miscible in the melt. The Flory-Huggins interaction parameter (χ) between H- and D-PCL segments was estimated. The hydroxyl groups in the PCL chain-ends were found to contribute significantly to the negative χ values. Combined characterization of small-angle X-ray scattering (SAXS) and small-angle neutron scattering (SANS) revealed that upon slow cooling, unique alternating H-rich and D-rich PCL lamellar structures are formed regardless of the blend ratio, which is attributed to the T_c difference between H- and D-PCLs. While upon rapid cooling, mixed crystals of H- and D-PCLs are predominantly formed. These results provide insightful information on the melt thermodynamics as well as detailed chain arrangements in lamellar crystals for semi-crystalline H/D polyester blends.

INTRODUCTION

Deuterium (D) labeling, in conjunction with neutron scattering, offers useful avenue for probing the chain structure and dynamics of semi-crystalline polymers.[2-6] The relevant investigations on polymer crystallization were often based on the assumption that protium (H)/D isotopic substitution has negligible effects on the thermodynamic interactions and polymer crystallization.[7, 8] However, studies have shown that deuterium substitution can affect the thermodynamics,[9-12] thermal properties,[13, 14] and crystal structures,[15] suggesting that it is crucial to consider the isotope effect in the corresponding data analysis for correctness. In the 1970s, this topic was extensively explored in H/D polyethylene (PE) isotopic blends. A common result was that under slow cooling, D chains segregate from H chains due to the difference in their crystallization temperature and kinetics.[16-19] More recently, a contrary finding was exposed in other polymer system, such as in H/D isotactic polypropylene (iPP) blends[20, 21] and H/D polyoxymethylene (POM) blends.[22] Co-crystallization was found in the H/D iPP blends upon an isothermal crystallization process continued longer than 50 minutes, exhibiting almost random distribution of the H and D chain stems in the crystallites.[21] Co-crystallization of H and D chains was also observed in the H/D POM blends, even when the sample was slowly cooled (2 °C/min) from the melt.[22] Thus, whether H/D chains coexist as stacked lamellae or crystallize separately in different lamellae upon different cooling conditions also depends on chemistry, which remains a question, for the blends of newly synthesized H/D polymers.

Among different types of polymers, semi-crystalline polyesters with polar groups are much less investigated. A detailed examination of a typical H/D isotopic polyester blend would provide key information to enrich the general understanding of the deuterium isotope effects. For this purpose, we picked poly(ε-caprolactone) (PCL) as a model system. As one of the most important semi-crystalline polyesters that can be easily melt-processed in industry, PCL and its blends are widely used in biomedical fields due to its excellent biocompatibility and bioresorbability.[23, 24] Examination of the melt thermodynamics and crystallization in PCL isotopic blends is of fundamental importance for characterizing the structure of PCL-based materials.

In this work, we prepared a series of H- and D-PCLs. The Flory-Huggins interaction parameter χ between H and D PCL chains was evaluated by fitting small-angle neutron scattering (SANS) data, through the random phase

approximation (RPA) model as well as the Zimm analysis. Thermal behaviors of the blends were examined by differential scanning calorimetry (DSC). Moreover, H/D chain arrangement and crystalline structures after slow and rapid cooling were inspected separately, using temperature-resolved SANS and synchrotron small-angle X-ray scattering (SAXS). Our results show that H and D chains are miscible in the melt while hydroxyl groups in the PCL chain-ends have a significant impact on the χ value. The crystallization of the blends highly depends on the cooling rate. In particular, we find that after slow cooling process, the long period of D lamellae is always twice that of mixed H and D lamellae, regardless of the blending ratio inside, providing cogent evidence of forming alternating H/D lamellar crystals. These results offer much-needed information on H/D chain arrangement in lamellae in semi-crystalline H/D isotopic polyester blends.

EXPERIMENTAL SECTION

Materials

All reagents were used as received from the suppliers without further purification unless otherwise noted. Anhydrous toluene, dichloromethane (DCM), chloroform and methanol were purchased from Fisher Scientific. $Sn(Oct)_2$ (92.5-100.0%), ε-caprolactone (99%), tetrabromomethane (CBr_4) (99%) and triphenylphosphine (PPh_3) (99%) were obtained from Sigma-Aldrich; 2-methylpropane-1,3-diol (99%) was obtained from Oakwood Chemical Inc.

Sample Preparation

Fully deuterated ε-caprolactone (CL-d10) was synthesized through the Baeyer-Villager oxidation of cyclohexanone-d_{10} as shown in Figure S1 and detailed synthesis procedures were reported in our recent study.[25] D-PCL was synthesized by ring-opening polymerization of CL-d10 as shown in Figure S1. In a typical procedure, CL-d10 (2.768 g, 22.283 mmol), 2-methylpropane-1,3-diol (15.6 mg, 0.173 mmol), and 0.8 ml $Sn(Oct)_2$ solution in anhydrous toluene (0.1 M) were added into a Schlenk flask under N_2 protection. After heating at 115 °C under N_2 atmosphere with stirring for 72 h, the resulting polymer was dissolved in DCM and precipitated twice with methanol to obtain the purified D-PCL, followed by drying in a vacuum oven at room temperature. The polymerization procedure of H-PCL was similar to the procedure for D-PCL, however, the polymerization was completed in 24 h. The ^{13}C NMR spectra of D-PCL and H-PCL are shown in Figures S2a and S2b, respectively.

To obtain the bromide (Br)-terminated PCL (PCL-Br), the above described hydroxyl (OH)-terminated PCL (250 mg, 0.02 mmol) and PPh_3 (26.5 mg, 0.08 mmol) were dissolved in 30 ml of anhydrous DCM under N_2 protection. Then, CBr_4 (21 mg, 0.08 mmol) was added into the above solution under N_2 atmosphere. After stirring at room temperature for 4 hours, the solution was concentrated with a rotary evaporator and the PCL-Br precipitated twice in methanol. The resulting PCL-Br was dried in a vacuum oven at room temperature before use.

All of the PCL blends were prepared by solution mixing of the respective polymer in chloroform solutions. The ratios of the H/D-PCL blends were set to 20/80, 50/50 and 80/20 (w/w).

Sample Characterization

^{13}C-NMR spectra were obtained on a Varian VNMRS 500 NMR spectrometer at 23 °C in $CDCl_3$ (77.23 ppm ^{13}C reference) using inverse-gated decoupling with a relaxation delay of 25 seconds. The average acquisition is about 1000 scans. The number average molar mass (Mn) and dispersity of polymers were measured from a size exclusion chromatography (SEC) system equipped with an Agilent 1260 infinity Isocratic HPLC pump, a multi-angle light scattering detector (DAWN HELEOS-II, Wyatt), and a refractive index detector (Optilab T-rEX, Wyatt). THF was the eluent (1 mL/min, at 35 °C). Absolute molar masses were calculated with the dn/dc values measured separately (Table 1).[25]

Differential scanning calorimetry (DSC) was conducted on a TA Instruments Q-2000 DSC equipped with an RCS90 air cooler. All the tests were performed under nitrogen flow and the instrument was calibrated with sapphire and indium standards. Polymer powders was loaded on to aluminum Hermatic pans. The Fourier-transform infrared (FTIR) spectra were collected at 4 cm^{-1} resolution power using a Bruker vertex 70 FTIR spectrometer equipped with a deuterated triglycine sulfate (DTGS) detector in the transmission mode.

The disk samples for SANS measurements were sandwiched between a pair of quartz plates with a 0.5 mm thickness aluminum split-ring washer at 90 °C, which were carried out on a Linkam hot stage (THMS600). Then, the samples were loaded to a Titania cell. The temperature resolved SANS were performed at the Bio-SANS instrument at the High-Flux Isotope Reactor, Oak Ridge National Laboratory. The sample-to-detector distance was set to 15.5 m at a wavelength of 6 Å and wavelength spread $\Delta\lambda/\lambda$ = 0.13. The available q range was 0.003 < q < 0.8 A^{-1}, where $q = (4\pi \sin\theta/\lambda)$, and 2θ is the scattering angle. A sample aperture of 12 mm diameter was used for providing a sufficient neutron scattering intensity in 3 minutes exposure. Raw SANS data were corrected for sample transmission and background radiation. Cooling and heating process during SANS measurements were controlled by a water bath and chiller. The real-time temperature of samples was detected by thermal couple inside Titania cells. When the samples measured in the melt state, beam opened after temperature becoming stable and keeping several minutes. In the slow cooling process when crystallization started, beam opened while the temperature was decreased continuously. The temperature presented in the paper was an average value.

For SAXS and wide-angle X-ray scattering (WAXS) measurements. Samples with a thickness of 0.5mm were prepared by compression-molding and then stuck by Kapton film. The slow and rapid cooling treatment were finished on Linkam hot stage before testing. SAXS and WAXS were conducted at the Advanced Photon Source (APS) of Argonne National Laboratories in sector 12-ID-B with X-ray energy of 14 keV. The 2D data collected with a Pilatus2M detector located at 3.6m downstream of the samples were converted to 1D using silver behenate as an angle standard. The beam size was 300×20 μm^2. Exposure time was typically 1s.

The lamellar thickness d_{SAXS} was calculated using 1D electron density correlation function, the intensity distribution is a Fourier transform of the correlation function related to the scattering object, including primarily the crystalline and amorphous phase in semi-crystalline polymers. The electron density correlation function is defined as[26, 27]

$$K(r) = \int_0^\infty 4\pi s^2 I(s) cos(2\pi sr) ds \qquad (1)$$

Where $s = 2\sin\theta/\lambda$, $I(s)$ the intensity function. The scattering curve can be extrapolated towards the zero angle and infinite angle, e.g., by using SAXSDAT program.[26]

RESULTS AND DISCUSSION

Considering that the degree of polymerization and dispersity of PCL are expected to have a significant influence on their crystallization behaviors,[28] great care was taken to ensure uniformity in the number of repeating units for both H- and D-PCL samples. The detailed results of the synthesized H-PCL and D-PCL are presented in Table 1. The substitution of protium with deuterium in PCL can be characterized by the vibration mode change in Fourier transform infrared (FTIR) spectra (cf. Figure S3). In the blends, FTIR intensity of C-H stretching bands (2945 and 2868 cm^{-1}) decreases while the intensity of C-D stretching bands (2216 and 2106 cm^{-1}) increases as the D content increases, confirming the different percentages of deuteration.

Table 1. Information of synthesized polymers.

Polymers	M_n (g/mol)	Molar mass per unit (g/mol)	Degree of Polymerization	Dispersity
H-PCL	10,900	114.14	96	1.29
D-PCL	12,500	124.21	100	1.16

Thermodynamic Interactions

SANS measurements were conducted to investigate the thermodynamic interactions between H- and D-PCL in the melt. Figure 1a shows the total scattering intensity I_{total} as a function of scattering vector q for the H/D samples at 86.2 °C. The incoherent background I_{inc}, visible in the high q region, is mostly induced by hydrogen and decreases with increasing the deuterium ratio. The coherent scattering intensity I_{coh} was obtained by subtracting I_{inc} (see an example calculation[29] in Figure S4) from I_{total}. The plots I_{coh} versus q are presented in Figure 1b. The maximum scattering intensity was observed in the H/D 50/50 blend sample, for it has the largest neutron scattering length density (SLD) contrast.[30] The scattering curves of all the H/D blends generally exhibit the characteristic feature of a homogenous mixture.[31] A small upturn was found in the low-q region (q < 0.008 $Å^{-1}$) for the H/D 20/80 sample. However, fitting to the Porod law, $I_{coh} \sim q^{-n}$, rendered an exponent value close to 2.5 (see insert in Figure 1b). The exponent near 2 suggests a homogenous system, while the exponent equal to 4 indicates a sharp interphase boundaries.[31] Thus, there was no obvious phase separation in the 20/80 sample.

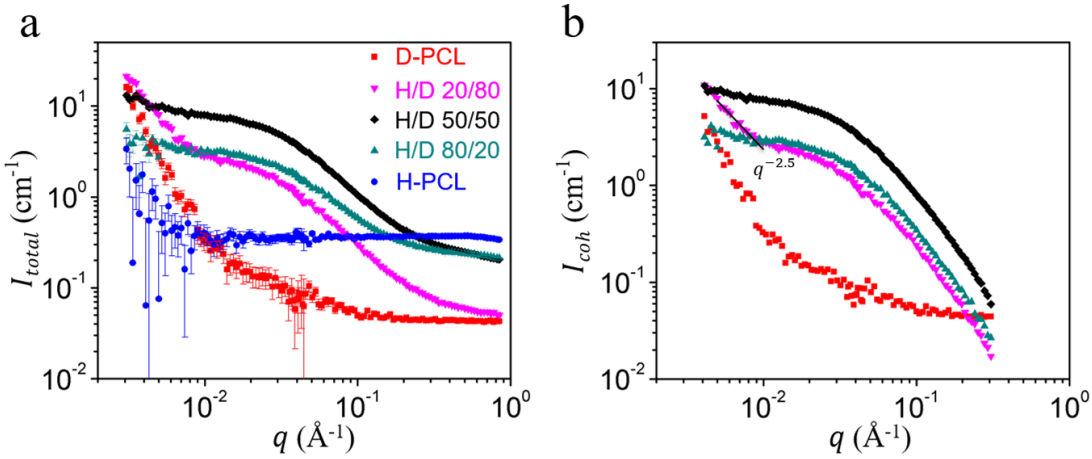

Figure 1. (a) SANS measurements of total scattering intensity I_{total} as a function of scattering vector q and (b) coherent scattering intensity I_{coh} *vs.* q for the H/D-PCL samples in the melt (86.2 °C). The I_{coh} *vs.* q curve of H-PCL sample is not presented since there was almost no coherent scattering.

The full range of the coherent scattering intensity I_{coh} versus q of H/D 50/50 was fitted using the random phase approximation (RPA) model.[32] From RPA, the Flory–Huggins interaction parameter χ was extracted to describe the interaction strength between H and D species.

$$S(q) = \frac{I_{coh}}{(b_H - b_D)^2 {v_0}^{-1}} \qquad (2)$$

$$\frac{1}{S(q)} = \frac{1}{(\phi_H N_H P_H)} + \frac{1}{(\phi_D N_D P_D)} - 2\chi_{RPA} \qquad (3)$$

where ϕ_i is the volume fraction, N_i is the degree of polymerization, and $i = H, D$. The scattering lengths are b_H = 1.41 ×10^{-12} cm and b_D = 11.82 × 10^{-12} cm for H and D chains, respectively. The reference monomer volume was chosen as $v_0 \approx v_H \approx v_D$ = 1.65 × 10^{-22} cm^3. P_i is the form factor given by the Debye function,[33]

$$P(u) = \frac{2(e^{-u}+u-1)}{u^2} \cong \frac{1}{1+u/3} \qquad (4)$$

where $u = q^2\langle {R_g}^2 \rangle$, and R_g is the radius of gyration of the polymer. For simplicity, R_g is assumed to be the same for H and D chains. The fitting parameters in the RPA model were χ_{RPA} and R_g. An example for the fitting of the SANS data at 54.5 °C is shown in Figure 2a. The fitted values of χ_{RPA} and R_g for various temperatures are presented in Figure 3 and Figure S5, respectively.

At small q range (the criterion of $qR_g \ll 1$ is met), Eq. 3 can be reduced to the Zimm equation,[29, 34, 35]

$$\frac{1}{S(q)} = \frac{1}{S(0)}(1 + \xi^2 q^2) \qquad (5)$$

$$\frac{1}{S(0)} = \frac{1}{(\phi_H N_H)} + \frac{1}{(\phi_D N_D)} - 2\chi_{Zimm} \qquad (6)$$

where ξ is the composition fluctuation correlation length and $\frac{1}{S(0)} = \frac{(b_H - b_D)^2 v^{-1}}{I_{coh}(q \to 0)}$ (based on Eq. 2). $I_{coh}(q \to 0)$ was obtained from fitting the Zimm plot, $I_{coh}{}^{-1}$ *vs.* q^2, as shown in Figure 2b, the intercept value of the linear fit with the ordinate was $I_{coh}{}^{-1}$ $(q \to 0)$ Calculated χ_{Zimm} at various temperatures are also presented in Figure 3.

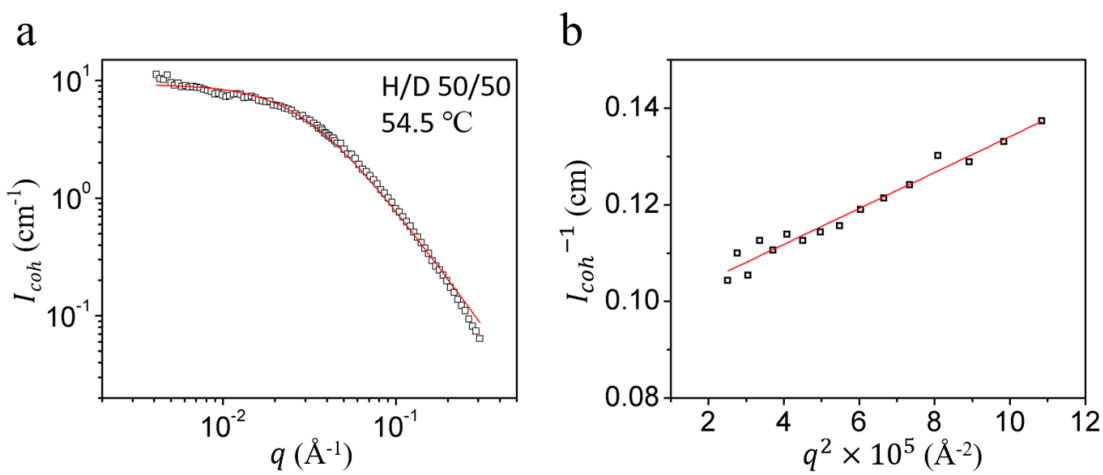

Figure 2. (a) SANS data showing I_{coh} *vs.* q (0.004-0.3 Å^{-1}) of the H/D 50/50 sample at 54.5 °C, solid line is the best fit of the RPA model; (b) Zimm plot, $I_{coh}{}^{-1}$ *vs.* q^2 for the H/D 50/50 sample at 54.5 °C, solid line represents the linear fit.

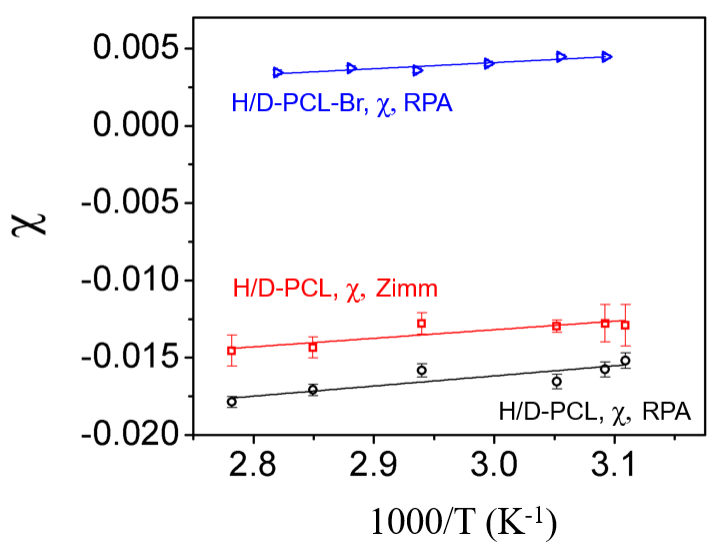

Figure 3. Flory-Huggins interaction parameter, χ, as a function of inverse temperature, fitted by the RPA model of H/D-PCL and H/D-PCL-Br samples and calculated from the Zimm analysis of H/D-PCL samples.

The temperature dependence of χ is given by $\chi_{RPA} = (6.56 \pm 1.74)/T - (0.036 \pm 0.0051)$ and $\chi_{Zimm} = (5.54 \pm 1.67)/T - (0.030 \pm 0.0049)$ respectively, *via* a linear fit of χ and T^{-1}. The χ_{RPA} and χ_{Zimm} values are rather close, and more importantly, both of sets are negative in the considered temperature range (and remain negative for the higher temperatures from the fitted equations). Negative χ values can be attributed to the effects of polar groups, small attraction irregularity (caused by similar solubility parameter[36, 37]), and more commonly, hydrogen bonding interaction, which is usually the dominant effect in systems with multiple hydrogen bonding sites, such as OH-terminated deuterated polystyrene/poly(butyl methacrylate) blend,[38] poly(2-vinylpyridine)/poly(4-hydroxystyrene) and poly(4-vinylpyridine)/poly(4-hydroxy-styrene) blends.[39]

To verify the non-trivial hydrogen bonding effect on thermodynamic interactions from even a few hydrogen bonding sites in H/D-PCL blends (between the chain-end group OH and the carbonyl or ether group), Br-terminated H- and D-PCLs (PCL-Br) were synthesized for a control study. H/D-PCL-Br 50/50 and H-PCL-Br/D-PCL 50/50 blends were prepared. The SANS curves of these samples are shown in Figure 4. In contrast to the OH-terminated H/D-PCL samples, two kinds of asymptotic behaviors were observed in the blends with Br-terminated PCLs. Specifically, the RPA behavior was found in the high-q region, whereas in the low-q region ($q < 0.006$ Å^{-1}), it exhibited the Debye-Bueche (DB) behavior as the Porod exponent of H/D-PCL-Br 50/50 sample is close to 4, indicating the existence of local inhomogeneities in the melt due to thermal fluctuations.

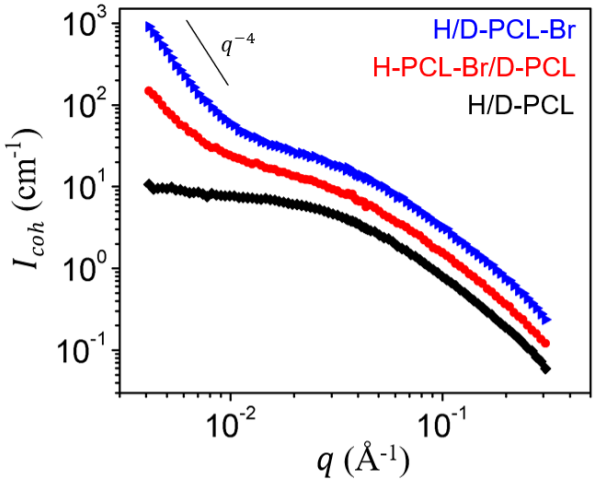

Figure 4. Coherent scattering intensity I_{coh} as a function of scattering vector q from SANS measurements for the H/D-PCL (86.2 °C), H-PCL-Br/D-PCL (82.0 °C) and H/D-PCL-Br (81.5 °C) 50/50 blends in the melt. Curves are vertically offset for clarity.

To obtain the χ values of H/D-PCL-Br 50/50 blend, we subtracted the DB type scattering behavior from the scattering curve and fitted the q > 0.015 Å^{-1} region to the RPA model. The χ results are presented in Figure 1d, with the fitted temperature dependence given by $\chi_{RPA} = (4.00 \pm 0.74)/T - (0.0079 \pm 0.0022)$. In general, H/D-PCL-Br 50/50 presented small positive χ values while the segregation strength $\chi N \ll 2$, indicating that the Br-terminated H/D-PCL blends are also miscible in the melt. Comparatively, the positive χ reflects the chain-end group impact in the OH-terminated H/D-PCL blends. These results essentially suggest that the effective negative χ in the H/D-PCL is composed of "bare" polymer interaction and hydrogen bonding interaction. Furthermore, a small amount of hydrogen bonding sites from chain-end groups could significantly enhance the blend miscibility. We note that this contribution was often omitted before, as the hydrogen bonding sites on the main chain were believed to be more important, especially when the polymers have large molar mass.

Crystallization Behavior and Chain Arrangement

The thermal behaviors of H/D-PCL blends were examined by DSC. The thermograms in Figure 5a show the results from slow cooling (0.5 ºC/min) process after removing thermal history. The subsequent heating curves are

presented in Figure 5b. An appropriate heating rate of 10 ºC/min was applied to prohibit the otherwise possible crystal thickening during slow heating and thermal lag in rapid heating.[40, 41] Single melting and crystallization peaks were observed. The crystallization temperature (T_c) and the melting point (T_m) are determined from the peak positions. The melting endothermic and exothermic peaks shifted toward the lower temperature side with increasing mass ratio of deuteration. Melting point depression by deuterated polymers can be attributed to the weaker intermolecular interactions resulting from the smaller polarizability of the C-D bond.[1, 13, 25, 42] The relative rapid cooling (20 ºC/min) and subsequent heating curves for the samples are shown in Figure 5c and 5d, respectively. Extra melting shoulders (indicated by arrows) were observed, owing to the melting of the cold-crystallized phase which is common after fast crystallization in semi-crystalline polymers including PCL.[43] The similar trend of the continuous change in T_m and T_c as a function of deuteration mass ratio was reported by Tashiro et al. in both H-iPP/D-iPP and H-POM/D-POM blend systems.[44, 45] The linear change of T_m and T_c with respect to the H/D ratio was interpreted as an evidence for the co-crystallization of H/D polymers, as H and D chains were found either statistically or randomly coexisting within the same lattice.[44, 45] Nevertheless, we note that DSC data alone is not sufficient to elucidate the co-crystallization behavior. Given the substantial T_c difference between H and D species in the H/D-PCL samples, the segregation between two components may occur during the slow cooling process (see illustration in Figure S7).

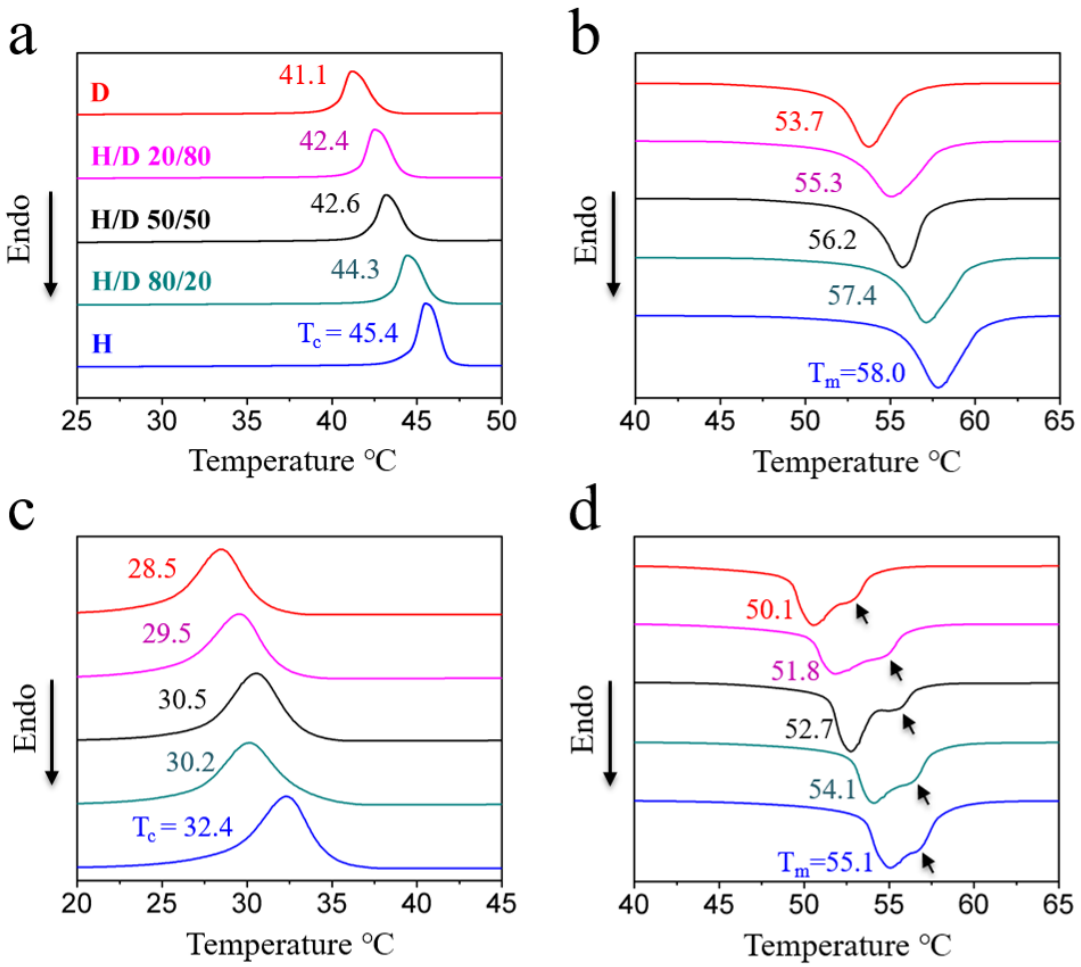

Figure 5. DSC (a) cooling curves at rate 0.5 ºC/min from the melt, (b) heating curves at rate 10 ºC /min after slow cooling (0.5 ºC/min) crystallization, (c) cooling curves at rate 20 ºC/min from the melt and (d) heating curves at rate 10 ºC /min after rapid cooling (20 ºC/min) crystallization of H-PCL, H/D 80/20, H/D 50/50, H/D 20/80 and D-PCL samples (from bottom to upper). Curves are vertically offset for clarity.

The crystal morphologies after slow and rapid cooling were explored. For PCL bulk crystallization, spherulites are the most common micro-scale structure.[46] The morphologies of spherulites in H/D-PCL blends can be found in Figure S8. In general, spherulites consist of lamellar polymer crystals. The lamellar structure was investigated using synchrotron SAXS and WAXS. The scattering profiles are shown in Figure S9. In Figure 6a, Lorentz-corrected SAXS profiles showed typical pattern of lamellar structure for the slow cooled samples (as expected for semi-crystalline polymers). The long period L of the lamellar structure can be calculated according to $L=2\pi/q^*$ from the primary peak positions q^* near 0.045 $Å^{-1}$. The values for the examined samples are summarized in Table

2. (The peak near q = 0.12 Å^{-1} was discussed in the supporting information). The lamellar thickness were calculated using the electron density correlation function Eq. 1 as described in the Sample Characterization section, the obtained $K(r)$ *vs.* r curves are showed in Figure 6b. After extrapolating the linear fragment to the intersection with the minimum level of the curves, we got the location of the first minimum of the crystalline-amorphous phase boundary.[20, 26] When the crystallinity of the sample is smaller than 50%, the location represents the statistic lamellar thickness; while the crystallinity is over 50%, the location means averaged amorphous thickness.[26] On the basis of the crystallinity of PCLs estimated from DSC measurement are over 50% (Table S1), we defined the first transition of the curves in Figure 6b as averaged amorphous thickness (L_{SAXS} - d_{SAXS}). Then, the volume crystallinity can be calculated according to d_{SAXS}/L_{SAXS} and the values are presented in Table 2. The long period L_{SAXS} and lamellar thickness d_{SAXS} in Table 2 show similar values for all the slow cooled samples (see Table S2 for the data of rapid cooled samples). H and D crystal unit cell dimensions only have slight difference indicated by WAXS as shown in Figure S9c, which is also discussed in detail in our previous report regarding pure D-PCL systems.[25] Therefore, we can conclude that the chain packing and the lamellar structure were almost unchanged with the presence of D-PCL chains.

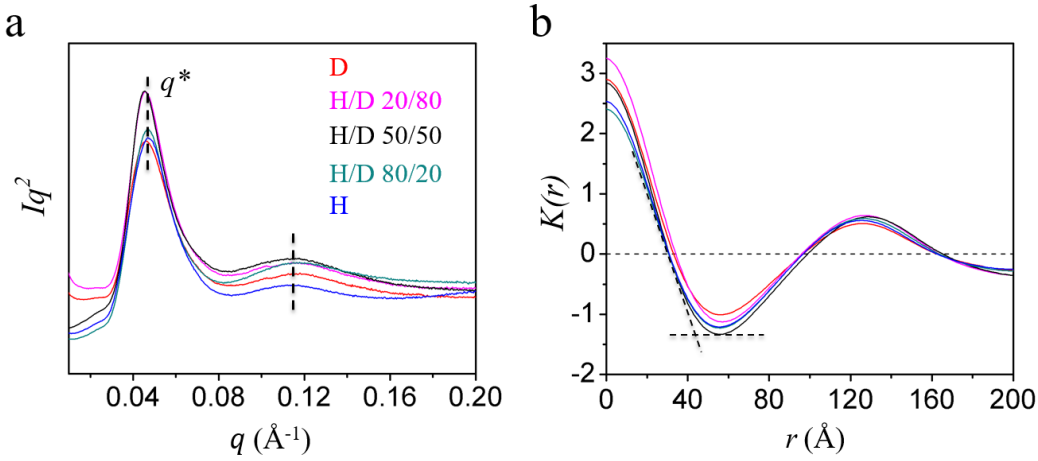

Figure 6. (a) Lorentz corrected SAXS profiles and (b) electron density correlation function curves for the H/D-PCL samples after slow cooling.

Different from SAXS (which is sensitive to variations in electron density), SANS is very sensitive to the hydrogen isotopic substitution, which can dramatically change the SLD. Figure 7a and 7b present the neutron coherent scattering intensities I_{coh} as a function of scattering vector q for the H/D-PCL samples after slow cooling and rapid cooling, respectively (I_{total} *vs.* q can be found in Figure S10). Neat D-PCL sample showed an obvious peak in both figures, indicating a long period L_{SANS} that is close to the value of L_{SAXS}. This peak stems from the contrast in neutron SLD between the amorphous phase (6.27×10^{-6} Å^{-2}) and the crystalline lamellar phase (6.81×10^{-6} Å^{-2}) of D-PCL, which is caused by the volumetric mass density difference between the amorphous phase (1.094 g/cm^3) and crystalline phase (1.187 g/cm^3).[47] By contrast, the structure information was not traceable in the SANS pattern for H-PCL, as the difference in SLD between its amorphous phase (0.81×10^{-6} Å^{-2}) and crystalline phase (0.88×10^{-6} Å^{-2}) is small while the incoherent background is relatively strong.

Table 2. Calculated SAXS and SANS data for H/D-PCL samples upon slow cooling

Samples	SAXS			SANS	L_{SANS}/L_{SAXS}
	Lamellar thickness d_{SAXS} (Å)	Long period L_{SAXS} (Å)	Volume crystallinity (%)	Long period L_{SANS} (Å)	
D-PCL	94.6	135.7	69.7	130.5	0.96
H/D 20/80	94.9	137.8	68.9	250.7	1.82
H/D 50/50	96.2	137.8	69.8	263.2	1.91
H/D 80/20	92.3	133.8	69.0	227.4	1.70
H-PCL	90.1	133.8	67.3	--	--

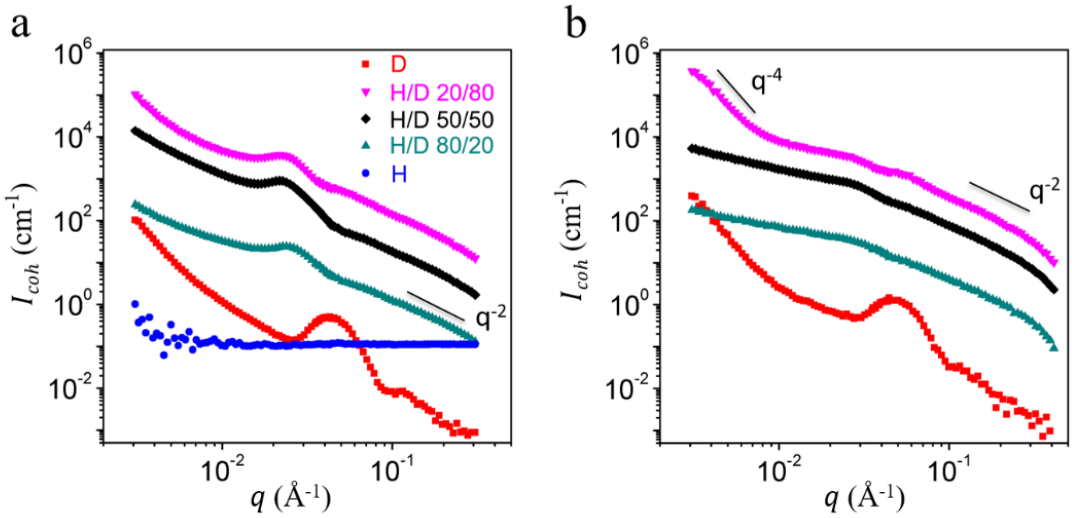

Figure 7. SANS measurements of coherent scattering intensity I_{coh} as a function of scattering vector q after (a) slow cooling and (b) rapid cooling (Curves are vertically shifted 10× for H/D 80/20, 100× for H/D 50/50 and 1000× for H/D 20/80 samples for clarity. Incoherent background of H-PCL sample was not removed since there was almost no coherent scattering).

For H/D blend samples, distinct peaks in the SANS scattering curves were observed after slow cooling; while after rapid cooling, only tiny peaks were found in the scattering profiles. The primary peaks can be attributed to the lamellar structures from crystallization, as they are absent in amorphous H/D blend samples.[10, 30] Lorentz-corrected SANS patterns are shown in Figure 8a. The long period L_{SANS} was calculated from the primary peak positions near q = 0.025 Å^{-1} and the results are presented in Table 2. The H/D 50/50 sample was found to have the strongest peak intensity and the largest long period. More importantly, the values of L_{SANS} for all the blend samples are about twice as long as the corresponding L_{SAXS}.

The two-fold relationship between L_{SANS} and L_{SAXS} of three blends is unique, implying that H and D species are separated during slow cooling crystallization process. It further excludes the possibility of randomly stacked H and D rich lamellae, as if this were the case, the L_{SANS} of 80/20 and 20/80 samples could be approximately 5 times larger than L_{SAXS} (as sketched in Figure S11). We propose that the factor of two between L_{SANS} and L_{SAXS} for all the blends comes from the configuration with alternating H-rich and D-rich lamellar structure. A schematic illustration of the structure, L_{SANS} and L_{SAXS} is given in Figure 9b. The higher T_c of the H component indicates that

H chains nucleate first during slow cooling. When H chains are being incorporated into H crystal, most D chains are remained in the melt state, resulting in the excess of D chains adjacent to each H crystal domain (Figure 9a). Subsequently, D chains start to nucleate between H-rich lamellae with temperature further decreases. The scattering curves from temperature-resolved SANS measurements of the H/D 50/50 upon slow cooling are shown in Figure 8b, the evolution of which corroborates our proposition. In particular, a shoulder (indicated by arrow) emerged in the scattering curve at 46.0 °C, which signifies to the onset of H-chain nucleation. Accordingly, this shoulder characterized the long period between H crystals and the surrounding H/D mixed amorphous phase. With further decreasing the temperature, a unimodal peak developed at 43.8 °C and became more obvious at 41.8 °C, which depicted the growth of H and D crystals. These stronger peaks were attributed to the large contrast between H and D rich crystals. The primary peak positions are both around 0.025 $Å^{-1}$, indicating the emergence of H/D alternating lamellae before the completion of crystallization. Moreover, in H/D 80/20 and 20/80 blends, the primary SANS peaks are also located near q = 0.025 $Å^{-1}$ (see Figure 8c and 8d), showing the similar feature. However, with increasing the deuterium content, the lamellar peaks occurred at lower temperatures, that corresponds well with the DSC results. For comparison, the isothermal crystallization of the H/D 50/50 at 46 °C was also examined by SANS, which exhibited the same H/D alternating lamellae structure (cf. Figure S12).

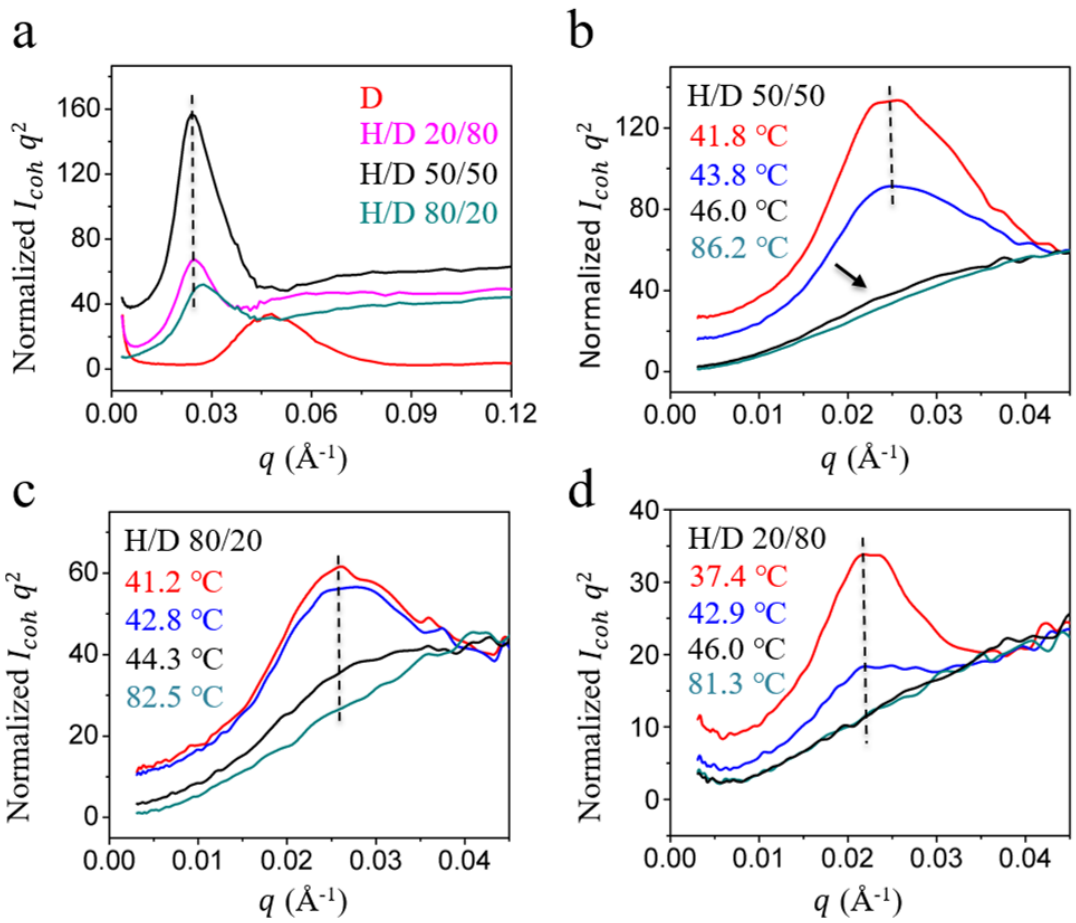

Figure 8. (a) Lorentz-corrected 1D SANS patterns, $I_{coh}\ q^2$ vs q for H/D-PCL samples after slow cooling. Temperature-resolved SANS patterns of (b) H/D 50/50, (c) H/D 80/20, and (d) H/D 20/80 during slow cooling. The primary peak positions are indicated by dotted lines.

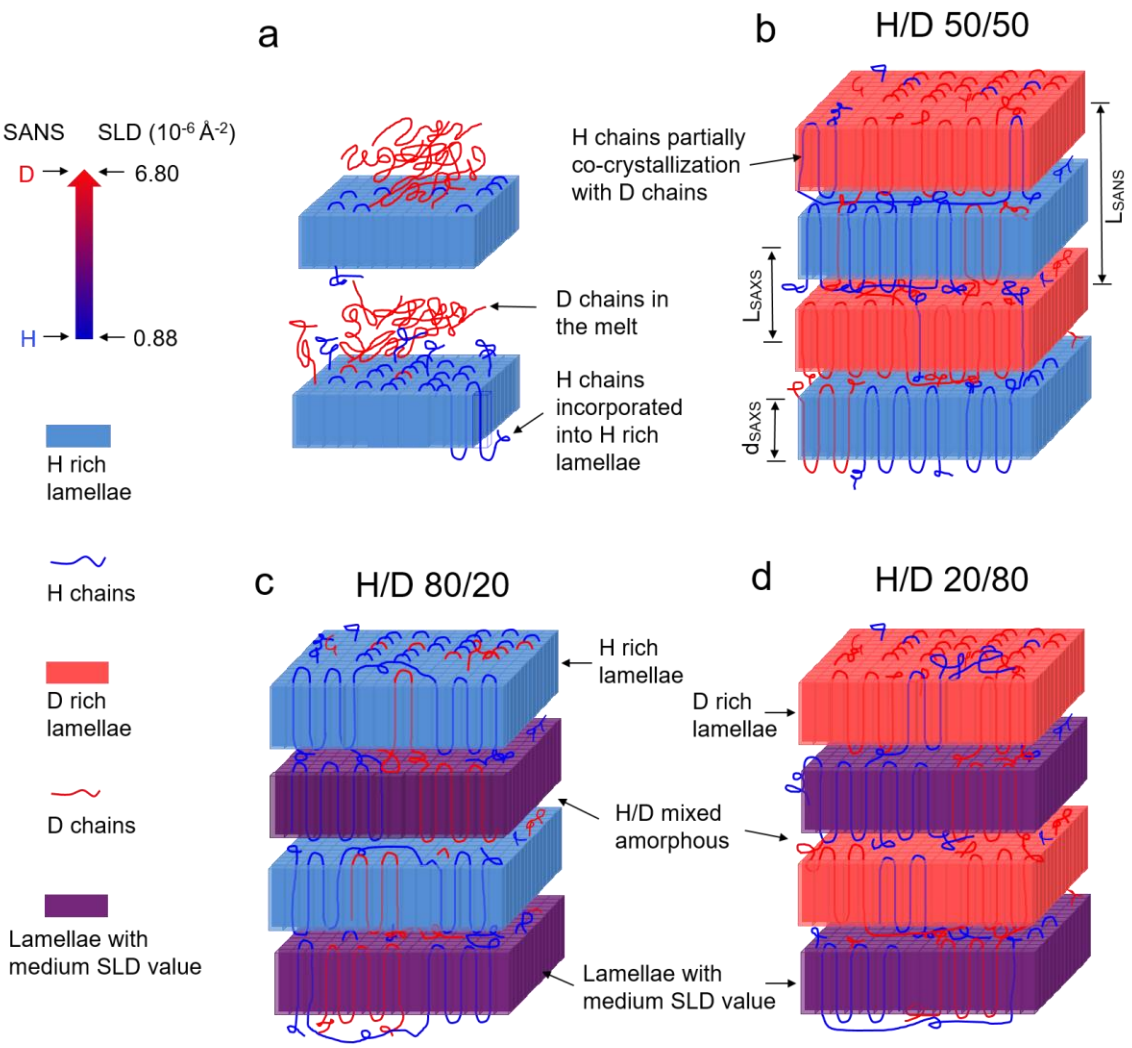

Figure 9. Schematic illustration model for (a) crystallization processing and final lamellar structure of (b) H/D 50/50, (c) H/D 80/20, (d) H/D 20/80. According to the theoretical models of crystallization updated by Miyoshi's group recently, both random re-entry and adjacent re-entry structures were drew in the model.[48-52]

A certain degree of mixing is expected that some H and D chains coexist within the same lamellae from slow cooling. This conjecture is supported by the fact that T_c and T_m were found to change continuously while only unimodal peaks in DSC curves were observed for all the samples. As the differences in T_c and T_m between neat H- and D-PCL samples are rather large, the unimodal DSC peak for the blend samples essentially suggests the formation of co-crystals by mixed H and D chains.[34, 44] The co-crystal lamellae should possess a medium SLD value between that of pure H and D in H/D 20/80 (20/80) due to the lack of H (D) chains. The SANS peaks in 80/20, 50/50, 20/80 blends can thus be attributed to the contrast between H-rich lamellae and co-crystal lamellae,

H-rich lamellae and D-rich lamellae, co-crystal lamellae and D-rich lamellae, respectively, as illustrated in Figure 9. Based on these schematic models, one would expect that H/D 50/50 has the largest peak due to the strongest contrast between the lamellar domains. Meanwhile, the L_{SANS} is always twice that of the neat D-PCL system as well as of the L_{SAXS}, regardless of the blend ratio. Therefore, the scattering data implies that H- and D-PCL chains can form into separated crystals as well as into co-crystals in the blends upon slow cooling, although they are miscible in the melt. During rapid cooling, H and D chains do not have enough time to diffuse and separate from each other that most H and D chains co-crystallize. As a result, there were no apparent lamellae peaks found in the SANS patterns in Figure 7b.

CONCLUSIONS

In summary, we have investigated the thermodynamic interaction and crystallization behavior in a series of H/D PCL blends by using DSC, SAXS and SANS measurements. Negative Flory-Huggins interaction χ parameters were extracted by fitting the melt scattering data to the RPA model and by using the Zimm analysis. The outcome from these two methods showed good consistency, indicating that H and D chains are miscible in the melt. The chain-end hydroxyl groups with a small number of hydrogen bonding sites were found to contribute significantly to the negative χ values.

As to the thermal and crystallization behaviors, the melting temperature T_m and crystallization temperature T_c shift continuously towards lower temperature with increasing the D component in the blend. Upon slow cooling, H and D polymer chains tend to crystallize separately into different lamellar domains, while the co-crystallization in the same lamellae also takes place, exhibiting a unique alternating stacked H and D lamellar structure. By contrast, blend samples showed a higher degree of co-crystallization from rapid cooling, which effectively prevents the formation of separated H and D crystals that might be ideal for the usage of deuterium labeling. These findings highlight that the difference in H and D chain kinetics plays an important role in the blend crystallization process. Overall, this study provides insightful information on the thermodynamics in the blends of protiated and deuterated semi-crystalline polyesters, as well as on the chain arrangement in lamellar crystals formed upon different cooling conditions.

Acknowledgement

The authors gratefully appreciate the support of the National Natural Science Foundation of China (NO. 51573063). L. Li thanks the Chinese Scholarship Council for its financial support. The polymers were synthesized at the Center for Nanophase Materials Sciences (CNMS) at the Oak Ridge National Laboratory (ORNL), which is a DOE Office of Science User Facility. Neutron scattering studies were performed at the CG-3 Bio-SANS instrument at the High-Flux Isotope Reactor (HFIR), ORNL, which is sponsored by the Office of Biological and Environmental Research, and the Scientific User Facilities Division, Office of Basic Energy Sciences, U.S. Department of Energy. This research used resources of the Advanced Photon Source, a U.S. Department of Energy (DOE) Office of Science User Facility operated for the DOE Office of Science by Argonne National Laboratory under Contract No. DE-AC02-06CH11357. We thank Dr. Changwoo Do and Dr. Wei-Ren Chen (SNS, ORNL) for helping with the calculated SANS curves (SI).

Supporting information

Synthesis procedure of deuterated ε-caprolactone and D-PCL (Figure S1); ^{13}C NMR data for H- and D-PCL samples (Figure S2); FTIR spectra (Figure S3); $q^4 I_{total}$ *vs.* q^4 (Figure S4); R_g values (Figure S5); RPA fitting to I_{coh} *vs.* q for H/D-PCL-Br (Figure S6); Crystallization models for H/D semi-crystalline polymer blends (Figure S7); Spherulites morphology observed by POM (Figure S8); SAXS and WAXS profiles (Figure S9); I_{total} *vs.* q after slow and rapid cooling (Figure S10); Model for randomly distributed H/D-PCL lamellaes (Figure S11); SANS patterns for H/D 50/50 after isothermal crystallization at 46 °C (Figure S12); Heat of fusion data of H-PCL (Table S1); Calculated SAXS data for H/D-PCL samples after rapid cooling (Table S2); Supporting information for the SAXS peak near q = 0.12 $Å^{-1}$.

Reference

[1] L. Li, D. Chang, M.M.L. Arras, W. Li, T. Li, J.K. Keum, P.V. Bonnesen, X. Peng, K. Hong, Isotope Effects on the Crystallization Kinetics of Selectively Deuterated Poly(ε-Caprolactone), Journal of Polymer Science Part B: Polymer Physics, 0.

[2] B. Hammouda, Probing Nanoscale Structures—The SANS Toolbox. Gaithersburg, MD: Natl Institute Standards Technology Center for Neutron Research; 2016, in.

[3] W. Chen, D. Liu, L. Li, Multiscale characterization of semicrystalline polymeric materials by synchrotron radiation X-ray and neutron scattering, Polymer Crystallization, (2018) 10043.

[4] H. Yang, D. Liu, J. Ju, J. Li, Z. Wang, G. Yan, Y. Ji, W. Zhang, G. Sun, L. Li, Chain Deformation on the Formation of Shish Nuclei under Extension Flow: An in Situ SANS and SAXS Study, Macromolecules, 49 (2016) 9080-9088.

[5] K. Cui, Z. Ma, N. Tian, F. Su, D. Liu, L. Li, Multiscale and Multistep Ordering of Flow-Induced Nucleation of Polymers, Chemical Reviews, 118 (2018) 1840-1886.

[6] C.R. López-Barrón, Y. Zeng, J.J. Schaefer, A.P. Eberle, T.P. Lodge, F.S. Bates, Molecular Alignment in Polyethylene during Cold Drawing Using In-Situ SANS and Raman Spectroscopy, Macromolecules, 50 (2017) 3627-3636.

[7] G.D. Wignall, Y.B. Melnichenko, Recent applications of small-angle neutron scattering in strongly interacting soft condensed matter, Reports on Progress in Physics, 68 (2005) 1761.

[8] G.D. Wignall, Small angle neutron and x-ray scattering, Physical Properties of Polymers Handbook, (2007) 407-420.

[9] J. Londono, A. Narten, G. Wignall, K. Honnell, E. Hsieh, T. Johnson, F. Bates, Composition dependence of the interaction parameter in isotopic polymer blends, Macromolecules, 27 (1994) 2864-2871.

[10] F. Bates, G.t. Wignall, W. Koehler, Critical behavior of binary liquid mixtures of deuterated and protonated polymers, Physical review letters, 55 (1985) 2425-2428.

[11] F. Bates, G. Wignall, S. Dierker, Phase behavior of amorphous binary mixtures of perdeuterated and normal 1, 4-polybutadienes, Macromolecules, 19 (1986) 1938-1945.

[12] F. Bates, G. Wignall, Non-ideal mixing in binary blends of perdeuterated and protonated polystyrenes, Macromolecules, 19 (1986) 932-934.

[13] F. Bates, H. Keith, D. McWhan, Isotope effect on the melting temperature of nonpolar polymers, Macromolecules, 20 (1987) 3065-3070.

[14] B.M. Habersberger, D.W. Baugh, Solvent and Polymer Stereochemistry Play Key Roles in Deuterium Exchange and Partial Racemization of Polypropylenes, Macromolecules, 51 (2018) 1290-1295.

[15] J. Jakowski, J. Huang, S. Garashchuk, Y. Luo, K. Hong, J. Keum, B.G. Sumpter, Deuteration as a Means to Tune Crystallinity of Conducting Polymers, The Journal of Physical Chemistry Letters, 8 (2017) 4333-4340.

[16] F.C. Stehling, E. Ergos, L. Mandelkern, Phase Separation in n-Hexatriacontane-n-Hexatriacontane-d74 and Polyethylene-Poly(ethylene-d4) Systems, Macromolecules, 4 (1971) 672-677.

[17] J. Schelten, D. Ballard, G. Wignall, G. Longman, W. Schmatz, Small-angle neutron scattering studies of molten and crystalline polyethylene, Polymer, 17 (1976) 751-757.

[18] D. Sadler, A. Keller, Trajectory of polyethylene chains in single crystals by low angle neutron scattering, Polymer, 17 (1976) 37-40.

[19] M. Bank, S. Krimm, Mixed crystal infrared study of chain segregation in polyethylene, Journal of Polymer Science Part B: Polymer Letters, 8 (1970) 143-148.

[20] K.R. Reddy, K. Tashiro, T. Sakurai, N. Yamaguchi, S. Sasaki, H. Masunaga, M. Takata, Isothermal crystallization behavior of isotactic polypropylene H/D blends as viewed from time-resolved FTIR and synchrotron SAXS/WAXD measurements, Macromolecules, 42 (2009) 4191-4199.

[21] K.R. Reddy, K. Tashiro, T. Sakurai, N. Yamaguchi, Isotope effect on the isothermal crystallization behavior of isotactic polypropylene blends between the deuterated and hydrogenated species, Macromolecules, 42 (2009) 1672-1678.

[22] T. Kongkhlang, K.R. Reddy, T. Kitano, T. Nishu, K. Tashiro, Cocrystallization phenomenon of polyoxymethylene blend samples between the deuterated and hydrogenated species, Polymer journal, 43 (2011) 66-73.

[23] M.A. Woodruff, D.W. Hutmacher, The return of a forgotten polymer—Polycaprolactone in the 21st century, Progress in Polymer Science, 35 (2010) 1217-1256.

[24] T.K. Dash, V.B. Konkimalla, Poly-ϵ-caprolactone based formulations for drug delivery and tissue engineering: A review, Journal of Controlled Release, 158 (2012) 15-33.

[25] D. Chang, T. Li, L. Li, J. Jakowski, J. Huang, J.K. Keum, B. Lee, P.V. Bonnesen, M. Zhou, S. Garashchuk, B.G. Sumpter, K. Hong, Selectively Deuterated Poly(ε-caprolactone)s: Synthesis and Isotope Effects on the Crystal Structures and Properties, Macromolecules, 51 (2018) 9393-9404.
[26] S. RABIEJ, M. RABIEJ, Determination of the parameters of lamellar structure of semicrystalline polymers using a computer program SAXSDAT, Polimery, 56 (2011).
[27] J. Yang, Y. Liang, J. Luo, C. Zhao, C.C. Han, Multilength Scale Studies of the Confined Crystallization in Poly (l-lactide)-block-Poly (ethylene glycol) Copolymer, Macromolecules, 45 (2012) 4254-4261.
[28] A. Wurm, E. Zhuravlev, K. Eckstein, D. Jehnichen, D. Pospiech, R. Androsch, B. Wunderlich, C. Schick, Crystallization and Homogeneous Nucleation Kinetics of Poly(ε-caprolactone) (PCL) with Different Molar Masses, Macromolecules, 45 (2012) 3816-3828.
[29] J. Qiu, K.I. Mongcopa, R. Han, C.R. López-Barrón, M.L. Robertson, R. Krishnamoorti, Thermodynamic Interactions in a Model Polydiene/Polyolefin Blend Based on 1, 2-Polybutadiene, Macromolecules, 51 (2018) 3107-3115.
[30] A.-S. Robbes, F. Cousin, F. Meneau, J. Jestin, Melt Chain Conformation in Nanoparticles/Polymer Nanocomposites Elucidated by the SANS Extrapolation Method: Evidence of the Filler Contribution, Macromolecules, 51 (2018) 2216-2226.
[31] T.J. Shin, B. Lee, B.S. Seong, Y.S. Han, C.-H. Lee, H.H. Song, R.S. Stein, M. Ree, Composition-dependent phase segregation and cocrystallization behaviors of blends of metallocene-catalyzed octene-LLDPE (D) and LDPE (H), Polymer, 51 (2010) 5799-5806.
[32] R. Alamo, J. Londono, L. Mandelkern, F. Stehling, G. Wignall, Phase behavior of blends of linear and branched polyethylenes in the molten and solid states by small-angle neutron scattering, Macromolecules, 27 (1994) 411-417.
[33] X. Chen, G.D. Wignall, L. He, C. Lopez-Barron, R.G. Alamo, SANS Evidence of Liquid–Liquid Phase Separation Leading to Inversion of Crystallization Rate of Broadly Distributed Random Ethylene Copolymers, Macromolecules, 50 (2017) 4406-4414.
[34] G. Wignall, J. Londono, J. Lin, R. Alamo, M. Galante, L. Mandelkern, Morphology of blends of linear and long-chain-branched polyethylenes in the solid state: a study by SANS, SAXS, and DSC, Macromolecules, 28 (1995) 3156-3167.
[35] K. Tashiro, K. Imanishi, M. Izuchi, M. Kobayashi, Y. Itoh, M. Imai, Y. Yamaguchi, M. Ohashi, R.S. Stein, Cocrystallization and phase segregation of polyethylene blends between the D and H species. 8. Small-angle neutron scattering study of the molten state and the structural relationship of chains between the melt and the crystalline state, Macromolecules, 28 (1995) 8484-8490.
[36] R. Krishnamoorti, W. Graessley, L. Fetters, R. Garner, D. Lohse, Anomalous mixing behavior of polyisobutylene with other polyolefins, Macromolecules, 28 (1995) 1252-1259.
[37] G.C. Reichart, W.W. Graessley, R.A. Register, R. Krishnamoorti, D.J. Lohse, Anomalous Attractive Interactions in Polypropylene Blends, Macromolecules, 30 (1997) 3036-3041.
[38] C. Zhou, E.K. Hobbie, B.J. Bauer, L. Sung, M. Jiang, C.C. Han, Control of Interaction Strength in Hydrogen-Bonded Polymer Blends via the Density of the Hydroxyl Group, Macromolecules, 31 (1998) 1937-1941.
[39] J. Kwak, S.H. Han, H.C. Moon, J.K. Kim, V. Pryamitsyn, V. Ganesan, Effect of the Degree of Hydrogen Bonding on Asymmetric Lamellar Microdomains in Binary Block Copolymer Blends, Macromolecules, 48 (2015) 6347-6352.
[40] H. Marand, J.D. Hoffman, Determination of the fold surface free energy and the equilibrium melting temperature for. alpha.-phase poly (pivalolactone) crystals, Macromolecules, 23 (1990) 3682-3687.
[41] E. Hellmuth, B. Wunderlich, Superheating of Linear High‐Polymer Polyethylene Crystals, Journal of Applied Physics, 36 (1965) 3039-3044.
[42] D.J. Lacks, Origins of molar volume isotope effects in hydrocarbon systems, The Journal of chemical physics, 103 (1995) 5085-5090.
[43] E. Zhuravlev, J.W.P. Schmelzer, B. Wunderlich, C. Schick, Kinetics of nucleation and crystallization in poly(ε-caprolactone) (PCL), Polymer, 52 (2011) 1983-1997.
[44] K.R. Reddy, K. Tashiro, T. Sakurai, N. Yamaguchi, Cocrystallization phenomenon between the H and D Species of isotactic polypropylene blends as revealed by thermal and infrared spectroscopic analyses for a series of D/H blend samples, Macromolecules, 41 (2008) 9807-9813.
[45] S. Kummara, K. Tashiro, T. Monma, K. Horita, Isotope Effect on the Melt–Isothermal Crystallization of Polyoxymethylene D/H Random Copolymers and D/H Blend Samples, Macromolecules, 48 (2015) 8070-8081.
[46] P.J. Phillips, G.J. Rensch, K.D. Taylor, Crystallization studies of poly (ε‐caprolactone). I. Morphology and kinetics, Journal of Polymer Science Part B: Polymer Physics, 25 (1987) 1725-1740.

[47] F. Khambatta, F. Warner, T. Russell, R. Stein, Small - angle x - ray and light scattering studies of the morphology of blends of poly (ϵ - caprolactone) with poly (vinyl chloride), Journal of Polymer Science Part B: Polymer Physics, 14 (1976) 1391-1424.
[48] Z. Li, Y.-l. Hong, S. Yuan, J. Kang, A. Kamimura, A. Otsubo, T. Miyoshi, Determination of Chain-Folding Structure of Isotactic Polypropylene in Melt-Grown α Crystals by 13C–13C Double Quantum NMR and Selective Isotopic Labeling, Macromolecules, 48 (2015) 5752-5760.
[49] Y.-l. Hong, T. Koga, T. Miyoshi, Chain trajectory and crystallization mechanism of a semicrystalline polymer in melt- and solution-grown crystals as studied using 13C–13C double-quantum NMR, Macromolecules, 48 (2015) 3282-3293.
[50] Y.-l. Hong, T. Miyoshi, Chain-Folding Structure of a Semicrystalline Polymer in Bulk Crystals Determined by 13C–13C Double Quantum NMR, ACS Macro Letters, 2 (2013) 501-505.
[51] Y.-l. Hong, W. Chen, S. Yuan, J. Kang, T. Miyoshi, Chain Trajectory of Semicrystalline Polymers As Revealed by Solid-State NMR Spectroscopy, ACS Macro Letters, 5 (2016) 355-358.
[52] S. Yuan, Z. Li, Y.-l. Hong, Y. Ke, J. Kang, A. Kamimura, A. Otsubo, T. Miyoshi, Folding of Polymer Chains in the Early Stage of Crystallization, ACS Macro Letters, 4 (2015) 1382-1385.